

# Electronic excitation spectra from *ab-initio* band structure results for $\text{LaMO}_3$ ( $M = \text{Cr-Ni}$ )

D. D. Sarma, N. Shanthi and Priya Mahadevan

*Solid State and Structural Chemistry Unit, Indian Institute of Science, Bangalore 560012, India*

(July 2, 2021)

## Abstract

We present calculated electron excitation spectra for the  $\text{LaMO}_3$  series ( $M=\text{Cr-Ni}$ ) obtained within *ab-initio* band structure calculations for the real geometric and magnetic structures. The calculated results show good agreement with the experimentally obtained spectra. This suggests that the transition metal-transition metal interactions via the oxygen atom play an important role in determining the spectroscopic features and indicates a smaller value of  $U/t$  than has been believed so far. The present approach undermines the importance of multiplet interactions which otherwise play an important role within various single impurity models.

PACS numbers: 71.20.-b, 71.27.+a, 75.10.Lp, 75.25.+z

## Introduction

During the last few years, a lot of attention has been focussed on the electronic structure of the  $3d$  transition metal oxides following the discovery of many exotic properties like high-temperature superconductivity [1], giant magnetoresistance [2] and other phenomena [3]. Many of these properties indicate a close interplay between magnetic and electronic properties. This arises from a simultaneous presence of strong electron-electron interaction strength,  $U$ , within the transition metal  $d$  manifold, and a sizable hopping interaction strength,  $t$  between the transition metal  $d$  and oxygen  $p$  states. While large values of  $U$  tend to localize the electrons and stabilize a magnetic moment at the transition metal site, the presence of large  $t$ , on the other hand, leads to a tendency towards delocalization of the electrons. Thus, this competition between the two opposing tendencies leads to the wide spectrum of electronic and magnetic ground states in transition metal oxides. Electron spectroscopies have played a very important role in understanding the electronic structure of such strongly correlated electron systems over more than a decade now. These spectroscopic results have been traditionally interpreted with the help of various single-impurity models, such as the cluster model [4] or the Anderson impurity model [5]. Within this approach, one considers only a single transition metal ion interacting with a cluster of oxygen atoms [4], or with a ligand derived  $p$ -band [5]. Thus, this model completely ignores the lattice periodicity of the transition metal site. It is reasonable to expect a negligible strength of direct hopping interaction between nearest neighbor transition metal sites owing to their large spatial separation in most of the oxides; however, two transition metal sites can still have a substantial effective interaction via the oxygen atom in between, if the transition metal  $d$  - oxygen  $p$  hopping interaction strength,  $t$  is large enough. Thus, it is obvious that a single impurity approach is expected to be most suitable in the limit of large  $U/t$ . While it is generally assumed to be the case, it is, however, not yet an established fact for *all* transition metal oxides.

In very recent times, there is a growing awareness that there may indeed be a strong coupling between the neighboring transition metal sites in many such compounds, making it

necessary to explore models that are more relevant to the electronic structure of transition metal oxides than a single-impurity model. For example, it has been recently shown that the spectral features of the prototypical examples of strongly correlated transition metal oxides, NiO and CuO [6] are better described within a multi-impurity model compared to single-impurity ones. More recently, it has been shown [7] that the ground state magnetic and electronic properties of  $\text{LaMO}_3$  compounds with  $M = \text{Mn-Ni}$  are correctly predicted by *ab-initio* band structure calculations. Furthermore, it was found that the *ab-initio* band structure approach also provided a reliable description of the x-ray photoelectron spectra of the valence band in  $\text{LaMO}_3$  with  $M=\text{Mn-Ni}$  [7]. In contrast, the traditional belief has been that band theory is a complete failure for the excitation spectra of every kind of transition metal compound and that it is necessary to describe the excitation spectra within models appropriate for strongly correlated systems, such as the Anderson impurity model. It is to be noted that the band theory and the Anderson impurity model represent two attempts to describe correlated systems from two different limits. While the band theory approach provides an accurate and *ab-initio* description of various hopping interaction strengths in the lattice, it treats the Coulomb interaction only in an approximate and average effectively single particle sense. On the other hand, impurity hamiltonians ignore the lattice of the transition metal ions, while providing a rigorous though parametrized treatment of the intra-atomic Coulomb interaction. It is well-known that the impurity model approach has been satisfactory in general in describing a variety of excitation spectra of a large number of transition metal compounds. On the other hand, the success of band theory to describe the excitation spectra of  $\text{LaMO}_3$  compounds with  $M=\text{Mn-Ni}$  [7] has been demonstrated only for the x-ray valence band photoemission spectra. It is to be noted that such spectra are related only to the occupied parts of the electronic structure. In view of these considerations, the unexpected success of the band theory in this context is worth a closer inspection, since there are certain obvious merits in an *ab-initio* approach compared to any parametrized model. Thus, it was felt necessary to investigate whether band theoretical approach would also describe the unoccupied parts of the electronic structure in the same compounds, thus

providing a unified and *ab-initio* description of excitation spectra related to the entire electronic structure of these compounds. In order to do this, here we report the calculated unoccupied spectra for  $M=\text{Cr-Ni}$  and compare these with corresponding Bremsstrahlung isochromat (BI) spectra which probe the unoccupied part. In a few cases, the experimental BI spectra do not provide a critical check for the calculated spectra due to experimental difficulties. In such cases, we compare the oxygen  $K$ -edge x-ray absorption (XA) spectra with the corresponding calculated ones, since XA spectra also probe the unoccupied part of the electronic states. Furthermore, we present new results for the x-ray photoemission (XP) spectrum of  $\text{LaCrO}_3$ , not presented earlier [7]. All these results are discussed in terms of spin-polarizations and orbital characters of the states.

## Method

*Ab-initio* LSDA calculations were carried out using linearized muffin-tin orbital (LMTO) method within the atomic sphere approximation (ASA) [8]. For the series of compounds investigated, no empty sphere was required to fulfil the volume-filling criterion. Semi-relativistic calculations with full self-consistency were obtained using  $s, p, d$  and  $f$  basis at each atomic sphere. The calculations were performed with 283 and 80 k-points in the irreducible parts of the Brillouin zones (BZ) of the rhombohedral and orthorhombic structures, corresponding to 1000 and 216 k-points over the full BZ. In order to obtain the calculated spectra, it is necessary to calculate the transition matrix elements, since the spectral features are substantially modified from the DOS due to the presence of strong variations in transition probabilities corresponding to states with different site and angular momentum characters as well as with energy. Thus, energy dependent matrix elements were calculated for each angular momentum  $l$  and site starting with the converged LMTO potentials for each site within the formalism of Winter *et al.* [9]. In order to obtain the calculated spectra, the site and  $l$ -projected DOS were weighted by these calculated matrix elements and suitably broadened with a Gaussian representing the resolution broadening and an energy dependent Lorentzian representing life-time effects. Since the oxygen  $K$ -edge x-ray absorption spectrum probes the oxygen  $p$ -character in the unoccupied DOS due to dipole selection rules,

only the unoccupied oxygen  $p$  partial DOS without any matrix element correction was taken into account in this case. The calculated spectra were rigidly shifted in energy to align the most intense peak with that of the experiment correcting for the underestimation of the band gap in local density approximation, as has been discussed earlier [7].

Every calculation was performed for the real crystal structure [10] and the observed magnetic ground state.  $\text{LaCrO}_3$  and  $\text{LaFeO}_3$  have twenty atoms in the  $\text{Pbnm}$  unit cells;  $\text{LaMnO}_3$  also has twenty atoms in the  $\text{Pnma}$  unit cell.  $\text{LaCoO}_3$  and  $\text{LaNiO}_3$  have ten atoms each in the  $\text{R}\bar{3}\text{c}$  structure. The magnetic structure for which calculations were performed for these oxides are  $A$ -type AF (Mn),  $G$ -type AF (Cr and Fe) and nonmagnetic (Co and Ni) according to the observed ground state magnetic structures.

## Results and discussion

We show the comparison of x-ray photoemission valence band spectrum of  $\text{LaCrO}_3$  and the corresponding calculated spectrum in Fig. 1. The experimental spectrum exhibits the most intense peak at about 6 eV with a shoulder at about 4.5 eV binding energy. Another peak is clearly observed at about 1.5 eV binding energy. The spectral intensity of this feature relative to the most intense peak at 6 eV is found to become weaker with decreasing photon energy. This indicates that the spectral feature at 1.5 eV is predominantly due to Cr states, while the main peak has more oxygen  $p$  character. The calculated spectrum shown in Fig. 1a is in very good agreement with the spectral feature at about 6 eV and the shoulder at about 4.5 eV both in terms of spectral features, widths, energy positions and relative intensities. However, the energy position of the Cr  $d$  related feature near 1.5 eV is underestimated by about 0.9 eV in the calculation, though the spectral shape, intensity and width appear to be reasonably well described. The Cr  $d$  and O  $p$  contributions to the calculated spectrum shown in Fig. 1a show that the experimental feature at about 1.5 eV is almost entirely contributed by Cr  $d$  states, while the oxygen  $p$  related intensity is the dominant contribution to the most intense peak and the shoulder at higher binding energy, in agreement with the dependence of the observed experimental intensity on photon energy. The calculated DOS and partial DOS suggest that the shoulder at about 4.5 eV arises primarily from non-bonding oxygen

$p$  states with minimal contribution from the Cr  $d$  states, while the most intense peak arises from bonding Cr  $d$ -O  $p$  interaction. This interpretation is supported by the distribution of Cr  $d$  intensity in the calculated spectrum in Fig. 1a between 3 and 8 eV. The spin polarization of Cr  $d$  contribution from one of the Cr-sites in the calculated spectrum shows a very strong polarization for the primarily Cr  $d$  related intensity between 0 and 2 eV; however, the extent of spin polarization is considerably weakened in the energy region of primarily oxygen  $p$  contribution between 3 and 8 eV. The strong spin-polarization of the Cr  $d$  related feature is easily understood in terms of the  $t_{2g\uparrow}^3$  configuration of Cr<sup>3+</sup>  $d^3$  state.

It was not possible to record the BI spectrum of LaCrO<sub>3</sub> due to severe charging problem arising from the wide band gap insulating state of the compound. Doping of 10% Sr in LaCrO<sub>3</sub> decreases the resistivity of the sample considerably. The spectral features of La<sub>0.9</sub>Sr<sub>0.1</sub>CrO<sub>3</sub> have been found to be very similar to that of LaCrO<sub>3</sub> in various photoemission spectra and we believe that the BI spectra of these two compounds are also similar. We show the wide scan BI spectra of La<sub>0.9</sub>Sr<sub>0.1</sub>CrO<sub>3</sub> in Fig. 2. The intense peak near 8 eV arises from La  $4f$  contribution, while the strongly distorted conduction band spectral features can be observed only as a shoulder between 2 and 6 eV. This illustrates the problem of extracting any detailed spectral feature of the conduction band in such compounds due to the overlap of very intense features in BI spectra at higher energies. We do not believe that any spectral decomposition in such a situation will be reliable in absence of any detailed knowledge of the spectral shape of other features and thus, we do not make any such attempt here. Instead we compare the calculated spectrum of the unoccupied state with the raw experimental results in Fig. 3a. The calculated spectrum exhibits a peak close to 4 eV in the Cr  $d$  derived states. The calculated feature agrees with the experimental spectrum as suggested in Fig. 3a by a vertical line. However, the superposed features arising from other states, for example La  $4f$  states, make the determination of the experimental peak position very uncertain. The spectral decomposition in terms of the Cr  $d$  and O  $p$  contributions (Fig. 3a) indicate that there is very little contribution from O  $p$ -derived states in the BI spectrum. The calculated peak at about 4 eV has more down-spin character, though the

up-spin contribution is also sizable (see Fig. 3b). The relative intensities of the spin-resolved contributions suggest the down-spin to be arising from the transitions into the  $t_{2g\downarrow}^0$  states, while the up-spin contribution in the same energy region arises from  $e_{g\uparrow}^0$  states. There is a second spectral feature related to Cr  $d$  states in the BI spectrum; this can be barely seen as an asymmetry in the low energy wing of the La  $4f$  signal at about 6 eV in Fig. 2. Our calculations show that it has substantial Cr  $d$  down-spin contributions, though other states such as La  $d$  also significantly contribute broad spectral features at this energy range. We interpret the Cr  $d$  contribution near 6 eV as arising from transitions into  $e_{g\downarrow}^0$  states in view of the spin-polarization of Cr  $d$  states in this energy range. The energy separation between the  $t_{2g\downarrow}$  and  $e_{g\downarrow}$  states is about 2.5 eV and is an approximate measure of the total crystal field splitting in  $\text{LaCrO}_3$ .

It is clear from Figs. 2 and 3 that the band theoretical approach to describe the unoccupied spectral features is severely restricted in the case of BI spectrum of  $\text{LaCrO}_3$  due to the presence of the intense La  $4f$  spectral contributions. In order to be more certain of the efficacy of this approach, we have compared the oxygen  $K$ -edge x-ray absorption spectrum of  $\text{La}_{0.9}\text{Sr}_{0.1}\text{CrO}_3$  with the broadened oxygen  $p$ -DOS of  $\text{LaCrO}_3$  over a wider energy range, since the oxygen  $K$ -edge absorption spectra probe the oxygen  $p$ -admixture in the unoccupied parts due to dipolar selection rules. The calculated results suggest that all the energy positions of various features in the calculation are systematically overestimated by about 25% compared to the experimentally observed ones. Such an overestimation is not unexpected in a linearized band structure approach, since the band structure equations are linearized near the mean energy of the *occupied* densities of states in order to obtain accurate descriptions of the potentials and various ground state properties. Similar effects have been observed while comparing the unoccupied states with experimentally obtained spectra of other compounds as well [11]. Thus, we have uniformly contracted the energy scale of the calculated results by 25% before comparing it to the experimentally obtained spectra in Fig. 4. In the same figure, we also show the spin-polarized Cr  $d$  partial DOS after broadening for comparison. The experimental spectrum clearly shows a peak at about 4 eV due to transitions arising

from  $t_{2g\downarrow}$  and  $e_{g\uparrow}$  states as evidenced from the spin-polarized Cr  $d$  state contributions. This is in good agreement with the BI spectra presented in Fig. 3. The spectral feature due to the  $e_{g\downarrow}$  state is seen at about 6.5 eV. The clearer emergence of these peaks in the oxygen  $K$ -edge spectrum compared to the BI spectrum in Fig. 2 is due to the near absence of La  $4f$  related states in the  $K$ -edge spectrum; La  $4f$  states have relatively small oxygen  $p$ -admixture in these compounds, while it dominates the BI spectrum. The calculated spectrum for oxygen  $K$ -edge absorption in Fig. 4 clearly shows the first peak arising from an oxygen  $p$ -admixture into the Cr  $t_{2g\downarrow}$  and  $e_{g\uparrow}$  states at the right energy position with correct spectral shape and width. The second feature in the calculated spectrum arises from the oxygen  $p$  admixture into the Cr  $e_{g\downarrow}$  states. The third spectral feature in the experiment and the calculation at about 8.5 eV arises mainly from oxygen  $p$ -admixture with La derived states with negligible Cr  $d$  contribution. While there is a good overall agreement between the experimental and calculated results, there is a discrepancy in terms of the relative intensities of the two peaks at about 6.5 and 8.5 eV. This arises from our neglect of matrix element effects in the oxygen  $K$ -edge absorption spectrum. It is to be noted that the feature at 6.5 eV arises from oxygen  $p$ -admixture with Cr  $d$   $e_{g\downarrow}$  states, while the higher energy feature at 8.5 eV is due to the admixture with La states; thus the matrix element effects may be expected to play some role. Overall it appears that the band structure results provide a satisfactory and *ab-initio* description of the x-ray absorption spectrum of this compound.

The BI spectrum of  $\text{LaMnO}_3$  is compared with the calculated spectrum in Fig. 5a. From this figure, it is obvious that the spectral shape, width and position are well described by the calculated result. The increasing intensity of the experimental spectrum above 3.5 eV arises from the tailing of the intense La  $4f$  state, as has already been discussed. We find that the BI spectrum is almost entirely dominated by Mn  $d$  derived states; this is a consequence of much larger matrix elements for these states compared to oxygen  $p$ -states. The spin-polarized contributions shown in Fig. 5b suggest a dominant contribution from down-spin states arising from transitions into  $t_{2g\downarrow}^0$  and  $e_{g\downarrow}^0$  states, though there is considerable up-spin



contribution in the first few electron-volts from transitions into  $e_{g\uparrow}^1$  state.

In the case of BI spectrum from  $\text{LaFeO}_3$ , we once again encounter the same difficulty as in the case of  $\text{LaCrO}_3$ , arising from the large band-gap and very insulating nature of this compound. The consequent charging effects lead to a broadening of various spectral features and an overlap of the La  $4f$  states from the higher energy side, strongly distorting the Fe  $d$ -related spectral features. However, the spectrum shown in Fig. 6a suggests the existence of two features, marked by vertical lines. The positions of these features are consistent with the calculated doublet features which are dominated by Fe  $d$  states due to matrix element effects. The first peak in the calculated spectrum corresponds to transitions into  $t_{2g\downarrow}$  state while the higher energy, weaker intensity feature corresponds to the  $e_{g\downarrow}$  state. The spin-polarized contributions in Fig. 6b suggest a nearly complete spin-polarization of the BI spectrum from each Fe sites due to the  $t_{2g\downarrow}^3 e_{g\downarrow}^2$  configuration of  $\text{Fe}^{3+}$  high-spin state. In order to further test the usefulness of the band structure approach in this case, we have also calculated the oxygen  $K$ -edge x-ray absorption spectrum, in the same way as it was done for  $\text{LaCrO}_3$ . We show the experimental and calculated spectra in Fig. 7, after contracting the energy scale of the calculated result by 25%, as before. The calculated spectrum is evidently in good agreement with the experimentally observed features. The spin-polarization of the Fe  $d$  states in the same energy interval shown in Fig. 7 shows a doublet feature with almost entirely down-spin character. The relative intensities of these two features clearly suggest that the low energy peak arises from the transitions into  $t_{2g}$  states, while the higher energy feature arises from  $e_g$  states, suggesting a crystal-field splitting of about 1.4 eV in  $\text{LaFeO}_3$ . It is interesting to note that while the intensity ratio of the two Fe  $d$  related features follow the expected degeneracy ratio between the  $t_{2g}$  and  $e_g$  states, the experimental as well as the calculated x-ray absorption spectra have nearly equal intensities in the two corresponding features. This arises from the fact that the oxygen  $p$  admixture in the primarily Fe  $d$  derived states, probed by  $K$ -edge XA spectroscopy, is substantially larger for the  $e_g$  symmetry arising from a correspondingly larger hopping interaction strength than that for the  $t_{2g}$  symmetry [12].

We compare the experimental and calculated BI spectra of  $\text{LaCoO}_3$  in Fig. 8. The experimental spectrum clearly shows a doublet feature, though the spectral features are strongly distorted by the overlap of signals from other states, such as La  $4f$ . The calculated result describes the doublet structure well in terms of energy positions and widths. The BI spectrum is found to be dominated by Co  $d$ -derived states. Since the band structure calculation was performed for the nonmagnetic ground state of  $\text{LaCoO}_3$ , there is no spin-polarization of the Co  $d$  band in this case. It is to be noted that the Co  $d$  spectral feature in the BI spectrum arises from the transition  $t_{2g}^6 e_g^0$  to  $t_{2g}^6 e_g^1$  and can give rise to only a single line within a single-impurity approach corresponding to the transition from  $^1A_{1g}$  to  $^2E_g$  and the spectral width will be resolution limited. In contrast, the spectral feature clearly suggests a two-peak structure with considerable energy spread. Within the present interpretation, the doublet feature and the spectral width reflect features in the density of states obtained from band structure calculations [14]. Likewise, the x-ray photoemission spectrum of  $\text{LaCoO}_3$  [15] shows a single narrow peak feature at 1 eV arising from the low-spin  $t_{2g}^6$  configuration of  $\text{Co}^{3+}$  ions in an octahedral site. The width of the signal, apart from the resolution broadening, is due to the bandwidth of the  $t_{2g}$  states arising from the Co-O-Co interactions. Within a single-impurity description [13], a photoemission transition from the  $^1A_{1g}$  ( $t_{2g}^6$ ) configuration can give rise to only a single line corresponding to a final state  $^2T_{2g}$  ( $t_{2g}^5$ ). Thus, the width of the spectroscopically observed feature will be limited only by the resolution function of the spectrometer. However, the width experimentally observed appears to be considerably larger, suggesting limitations of a single-impurity description also for the photoemission spectrum.

Fig. 9 shows the experimental and calculated BI spectra of  $\text{LaNiO}_3$ . The experimental spectrum exhibits a rather broad single peak feature which appears to be fairly well described by the calculation. However, the calculated spectral width appears to be somewhat larger than the experimentally observed one. One contributing factor to this mismatch is the systematic overestimation of unoccupied energies within the linearized method, as has already been discussed. However, we note that the existence of strong correlation effects

within the metallic conduction band derived from the interaction between Ni  $d$  and O  $p$  states, may also lead to a narrowing of the experimental feature.

The above results conclusively establish that the excitation spectra of  $\text{LaMO}_3$  compounds with  $M=\text{Cr-Ni}$  are well described by band calculations. In contrast, it is well known that band calculations do not provide the correct description for the excitation spectra of the corresponding  $\text{MO}$  compounds. Thus, the present results suggest that the  $U/t$  values are smaller in the  $\text{LaMO}_3$  compounds compared to the corresponding  $\text{MO}$  compounds. This suggestion is indeed supported by several analysis already available in the literature [16–19]. For example,  $U/t$  for NiO has been estimated to be 5.8 [16] and 5.3 [20] while the same for  $\text{LaNiO}_3$  has been estimated to be about 3.9 [18] and 2.5 [19]. Similarly, the  $U/t$  for MnO is about 6.4 [16] whereas the same for  $\text{LaMnO}_3$  is estimated to be 4.2 [16] and 1.8 [19]; for TiO it is 3.8 [16] and for  $\text{LaTiO}_3$  1.7 [16]. Thus, we find that the  $U/t$  for the  $\text{MO}$  compounds is always significantly higher (about 50-100%) than those for the  $\text{LaMO}_3$  compounds. This is probably the single most important reason why band theory provides a satisfactory description for the electronic structure of  $\text{LaMO}_3$ , while failing in the case of  $\text{MO}$  compounds.

In summary, we have compared various single-particle excitation spectra of  $\text{LaMO}_3$  compounds with  $M = \text{Cr-Ni}$  to those obtained from *ab-initio* band structure results. The calculated spectral features agree remarkably well with the experimental ones for the wide range of compounds investigated. The present results clearly establish the importance of a sizable hopping interaction between various transition metal sites mediated via the oxygen states. One of the main drawbacks in the present approach is a systematic overestimation of the energy positions of unoccupied spectral features by about 25%. We have attributed this to the use of the linearized method employed for band structure calculations which is expected to yield best results for the occupied states. The other limitation of the present description arises from a serious underestimation of the band gaps by the calculations. This necessitated the use of the single adjustable parameter of the present approach which allowed us to shift the calculated spectra rigidly in order to match a peak in the experimental spectra. In spite

of this limitation, the agreement between the experiment and calculation is convincing in view of the presence of the single adjustable parameter, while the relative energy positions, spectral intensities, widths and shapes are accurately described within an *ab-initio* method. The underestimation of the band gap in LSDA approaches is well-known to arise from an average local treatment of the many-body potential arising from electron-electron interactions and several methods have been suggested to rectify this [21]. However, it appears that the effect of the Coulomb interaction strength at the transition metal site on the spectroscopic feature, is not as strong in these trivalent compounds as in the divalent compounds of late *3d* transition elements arising from a lower value of  $U/t$  in the trivalent case. This is further supported by the near absence of any correlation induced satellite features in any of the x-ray photoemission spectra of this series, while intense satellite features are easily observed in such spectra of the *MO* series. Moreover, the spectral widths in the  $\text{LaMO}_3$  series appear to be dominated by band structure effects rather than multiplet interaction effects,

### **Acknowledgment**

D.D.S thanks Dr. M. Methfessel, Dr. A. T. Paxton, and Dr. M. van Schiljgaarde for making the LMTO-ASA band structure program available and Dr. S. Krishnamurthy for initial help in setting up the LMTO-ASA program. We also thank Drs. N. Hamada, H. Sawada and K. Terakura for several discussions and an earlier collaboration [7] that preceded this work. Dr. N. Shanthi thanks the CSIR, Government of India for the Research Associateship.

## REFERENCES

- [1] Bednorz J.G and Muller K.A, Z. Phys. B **64**, 189 (1986).
- [2] R. von Helmont, J. Wecker, B. Holzaphel, L. Schultz and K. Samwer, Phys. Rev. Lett **71**, 2331 (1993).
- [3] A. Asamitsu, Y. Moritomo, Y. Tomioka, T. Arima and Y. Tokura, Nature **373**, 407 (1995); Y. Okimoto, T. Katsufuji, T. Ishikawa, A. Urushibara, T. Arima and Y. Tokura, Phys. Rev. Lett **75**, 109 (1995).
- [4] A.Fujimori and F.Minami, Phys. Rev. B **30**, 957 (1984) .
- [5] H.Eskes and G. A. Sawatzky, Phys. Rev. Lett. **61**, 1415 (1988).
- [6] M. A. van Veenendaal and G. A. Sawatzky, Phys. Rev. Lett. **70**, 2459 (1993); M. A. van Veenendaal, H.Eskes and G. A. Sawatzky, Phys. Rev. B **47**, 11462 (1993).
- [7] D. D. Sarma, N. Shanthi, S. R. Barman, N. Hamada, H. Sawada and K.Terakura, Phys. Rev. Lett **75**, 1126 (1995).
- [8] O. K. Anderson, Phys. Rev. B, **12** 3060 (1975); O. K. Anderson and R. V. Kasowski, Phys. Rev. B, **4** 1064 (1971); O. K. Anderson, Solid State Commun **13**, 133 (1973).
- [9] H. Winter, P. J. Durham and G. M. Stocks, J. Phys. F **14**, 1047 (1984).
- [10] LaCrO<sub>3</sub>: C. P. Khattak and D. E. Cox, J. Appl Cryst **10**, 405 (1977); LaMnO<sub>3</sub>: J. B. A. A. Elemans, B. Van Larr, K. R. Van Der Veen, and B. O. Loopstra, J. Solid State Chem., **3**, 238 (1971); LaFeO<sub>3</sub>: M. Marezio and P. D. Dernier, Mater. Res. Bull., **6**, 23 (1971); LaCoO<sub>3</sub>: G. Thornton, B. C. Tofield and A. W. Hewat, J. Solid State Chem **61**, 301 (1986); LaNiO<sub>3</sub>: J. L. Garcia-Munoz, J. Rodriguez-Carvajal, P. Lacorre and J. B. Torrance, Phys. Rev. B, **46**, 4414 (1992).
- [11] Shubha Gokhale, S. R. Barman and D. D. Sarma, Phys. Rev. B, **52**, 14526 (1995).
- [12] A. Chainani, M. Mathew and D. D. Sarma, Phys. Rev. B **48**, 14818 (1993).

- [13] M. Abbate, J. C. Fuggle, A. Fujimori, L. H. Tjeng, C. T. Chen, R. Potze, G. A. Sawatzky, H. Eisaki and S. Uchida, Phys. Rev. B **47**, 16124 (1993).
- [14] D. D. Sarma and S. R. Barman, Solid State Sciences Vol. 119, *Spectroscopy of Mott Insulators and Correlated Metals*, edited by A. Fujimori and Y. Tokura (Springer-Verlag, Berlin, 1995) p. 126.
- [15] A. Chainani, M. Mathew and D. D. Sarma, Phys. Rev. B **46**, 9976 (1992); S. R. Barman and D. D. Sarma, Phys. Rev. B **49**, 13979 (1994).
- [16] T. Saitoh, A. E. Bocquet, T. Mizokawa and A. Fujimori, Phys. Rev. B **52**, 7934 (1995).
- [17] A. E. Bocquet, T. Mizokawa, K. Morikawa, A. Fujimori, S. R. Barman, K. Maiti, D. D. Sarma, Y. Tokura and M. Onoda, Phys. Rev. B (in press).
- [18] T. Mizokawa and A. Fujimori, Phys. Rev. B **51**, 12880 , (1995)
- [19] D. D. Sarma and A. Chainani, **111**, 208 (1994); A. Chainani, M. Mathew and D. D. Sarma, Phys Rev. B **47**, 15397 (1993); S. R. Barman, A. Chainani and D. D. Sarma, Phys. Rev. B **49**, 8475 (1994).
- [20] M. A. van Veenendaal and G. A. Sawatzky, Phys. Rev. Lett **70**, **2459** (1993).
- [21] **F. Manghi, C. Calandra and Stefano Ossicini, Phys. Rev. Lett. 73, 3129 (1994); F. Aryasetiawan and O. Gunnarsson, Phys. Rev. Lett. 74, 3221 (1995).**

## FIGURES

FIG. 1. (a) Experimental valence band x-ray photoemission spectrum (dots) of  $\text{LaCrO}_3$  compared with the calculated spectrum (solid line). The relative contributions from Cr  $d$  states (dash) and O  $p$  states (dash-dot) to the calculated spectrum are also shown. (b) The spin-polarized contributions of Cr  $d$  states from one of the Cr sites to the calculated spectrum is shown here; the solid line is the up-spin contribution, while dashes represent the down-spin contribution.

FIG. 2. A wide scan BI spectrum of  $\text{La}_{0.9}\text{Sr}_{0.1}\text{CrO}_3$  showing the intense La  $4f$  peak at about 8.5 eV and weak intensity features related to Cr  $d$  states below 7 eV.

FIG. 3. (a) Experimental BI spectrum of (dots)  $\text{La}_{0.9}\text{Sr}_{0.1}\text{CrO}_3$  compared with the calculated spectrum (solid line) for  $\text{LaCrO}_3$ . The relative contributions from Cr  $d$  states (dash) and O  $p$  states (dash-dot) to the calculated spectrum are also shown. (b) The spin-polarized contributions of Cr  $d$  states from one of the Cr sites to the calculated spectrum is shown here; the solid line is the up-spin contribution, while dashes represent the down-spin contribution.

FIG. 4. Experimental x-ray absorption spectrum (dots) of  $\text{La}_{0.9}\text{Sr}_{0.1}\text{CrO}_3$  at the oxygen  $K$ -edge compared with the calculated spectrum (solid line) for  $\text{LaCrO}_3$ . The broadened spin-polarized Cr  $d$  partial DOS are also shown: up-spin (dash) and down-spin (dash-dot).

FIG. 5. (a) Experimental BI spectrum (dots) of  $\text{LaMnO}_3$  compared with the calculated spectrum (solid-line). The relative contributions from Mn  $d$  states (dash) and O  $p$  states (dash-dot) to the calculated spectrum are also shown. (b) The spin-polarized contributions of Mn  $d$  states from one of the Mn sites to the calculated spectrum is shown here; the solid line is the up-spin contribution, while dashes represent the down-spin contribution.

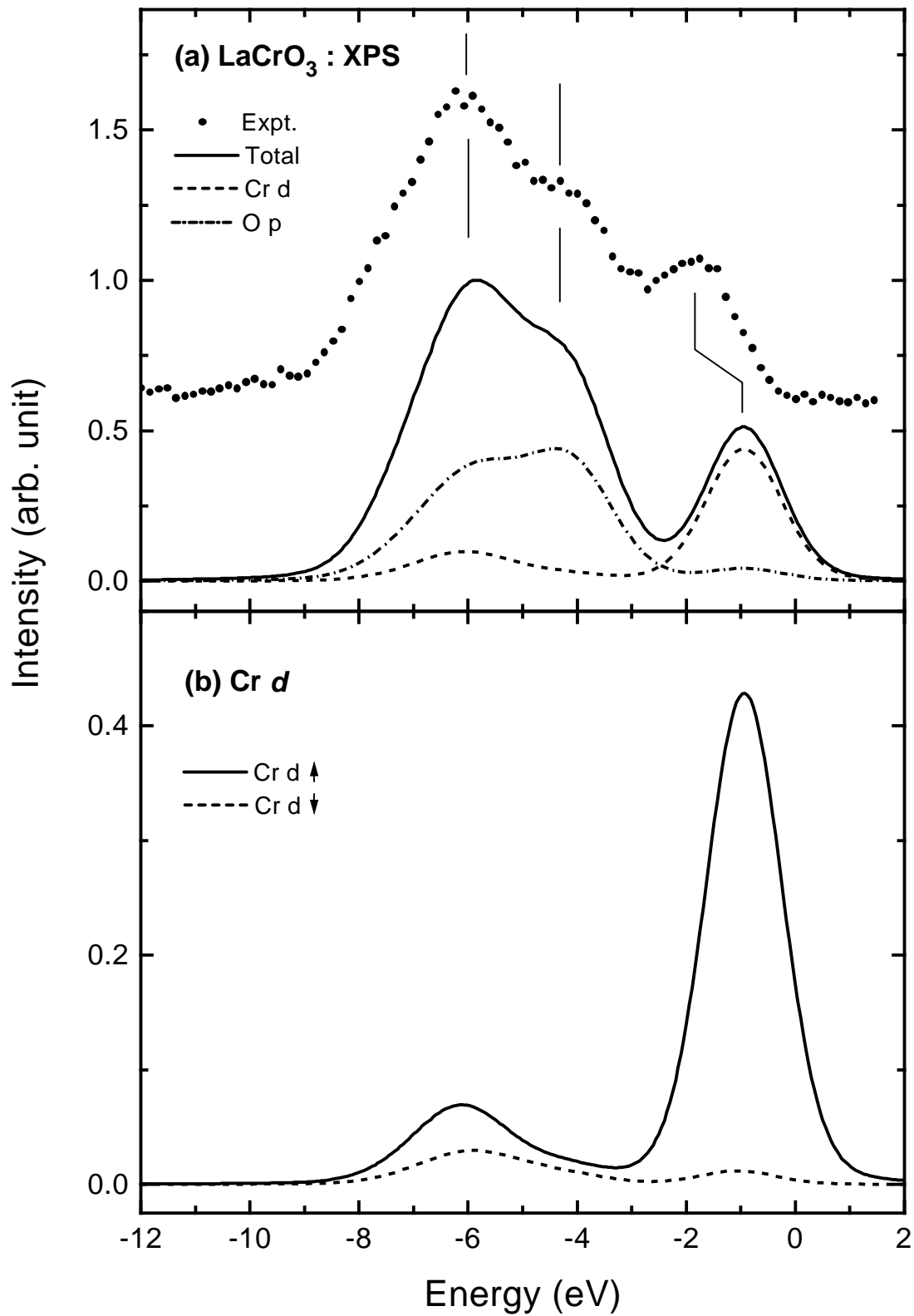
FIG. 6. Experimental BI spectrum (dots) of  $\text{LaFeO}_3$  compared with the calculated spectrum for  $\text{LaFeO}_3$  (solid line). The relative contributions from Fe  $d$  states (dash) and O  $p$  states (dash-dot) to the calculated spectrum are also shown. (b) The spin-polarized contributions of Fe  $d$  states from one of the Fe sites to the calculated spectrum is shown here; the solid line is the up-spin contribution, while dashes represent the down-spin contribution.

FIG. 7. Experimental x-ray absorption spectrum (dots) of  $\text{LaFeO}_3$  at the oxygen  $K$ -edge compared with the calculated spectrum (solid line) for  $\text{LaFeO}_3$ . The broadened spin-polarized Cr  $d$  partial DOS are also shown: up-spin (dash-dot) and down-spin (dash).

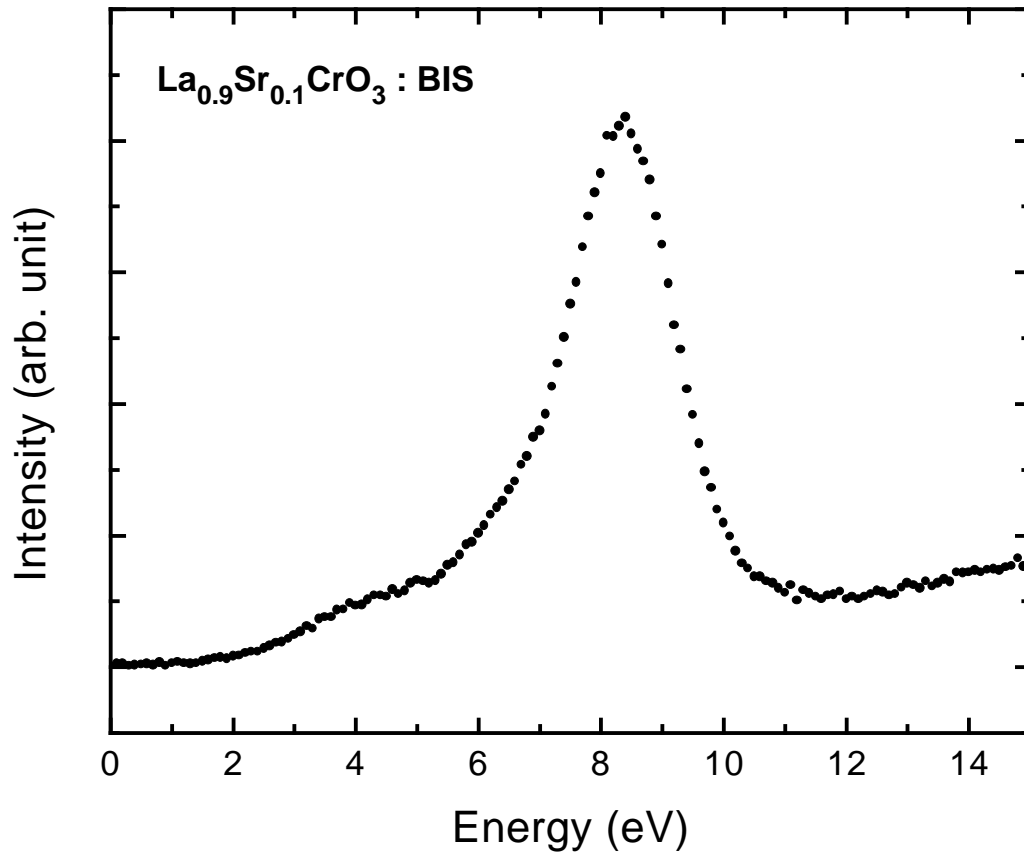
FIG. 8. Experimental BI spectrum (dots) of  $\text{LaCoO}_3$  compared with the calculated spectrum (solid line) for  $\text{LaCoO}_3$ . The relative contributions from Co  $d$  states (dash) and O  $p$  states (dash-dot) to the calculated spectrum are also shown.

FIG. 9. Experimental BI spectrum (dots) of  $\text{LaNiO}_3$  compared with the calculated spectrum (solid line) for  $\text{LaNiO}_3$ . The relative contributions from Ni  $d$  states (dash) and O  $p$  states (dash-dot) to the calculated spectrum are also shown.

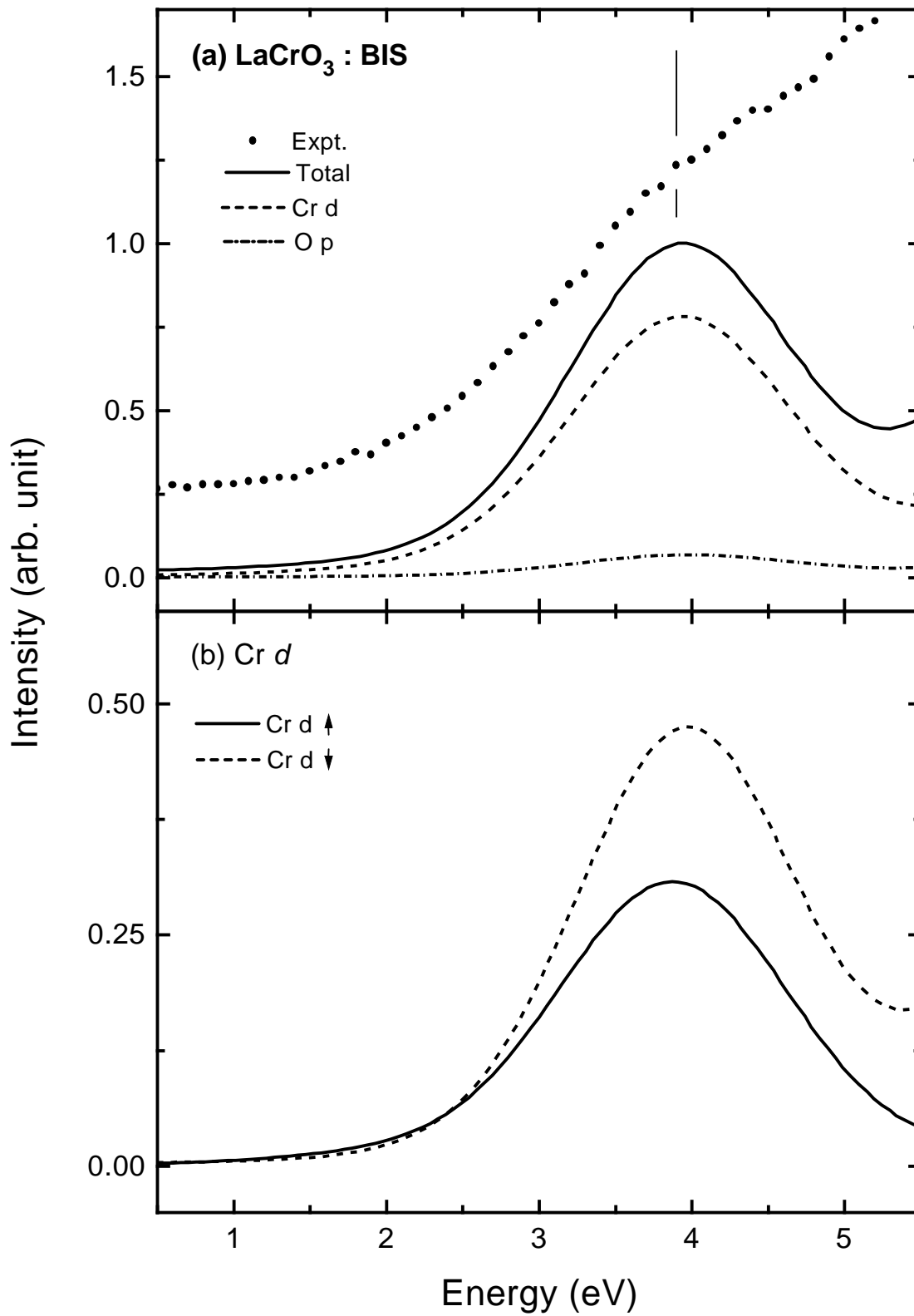




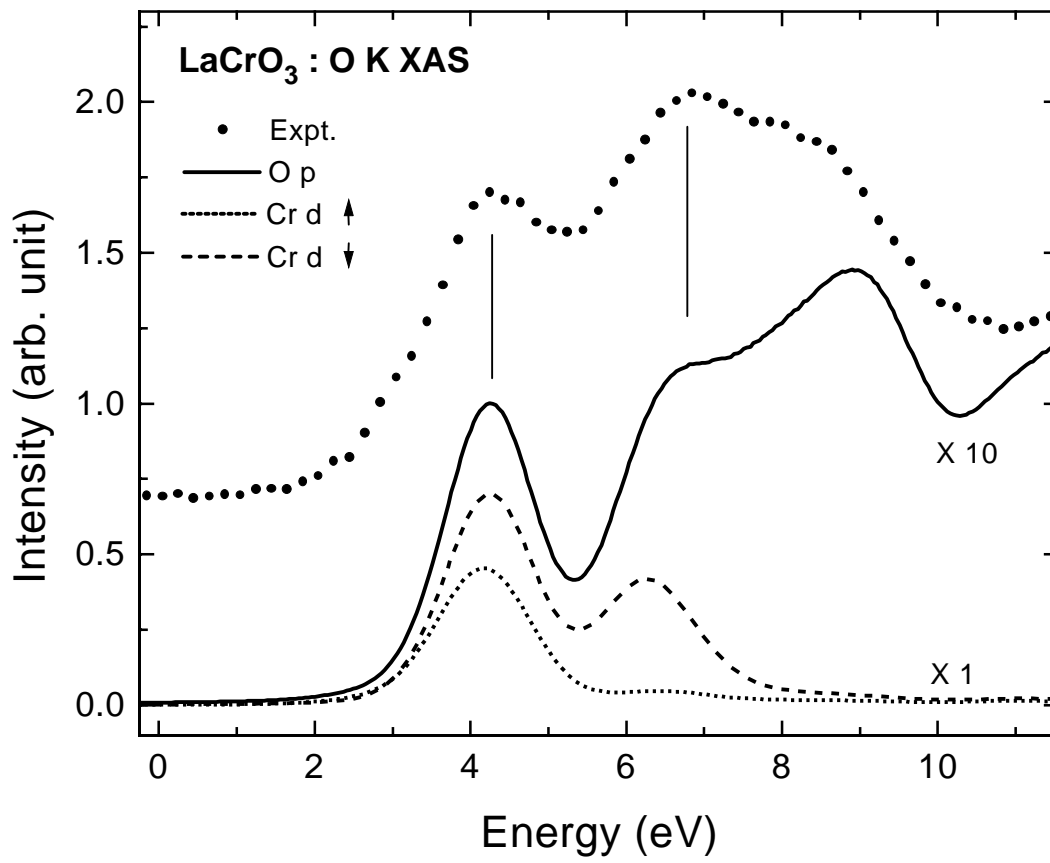
Sarma *et al.* Fig. 1



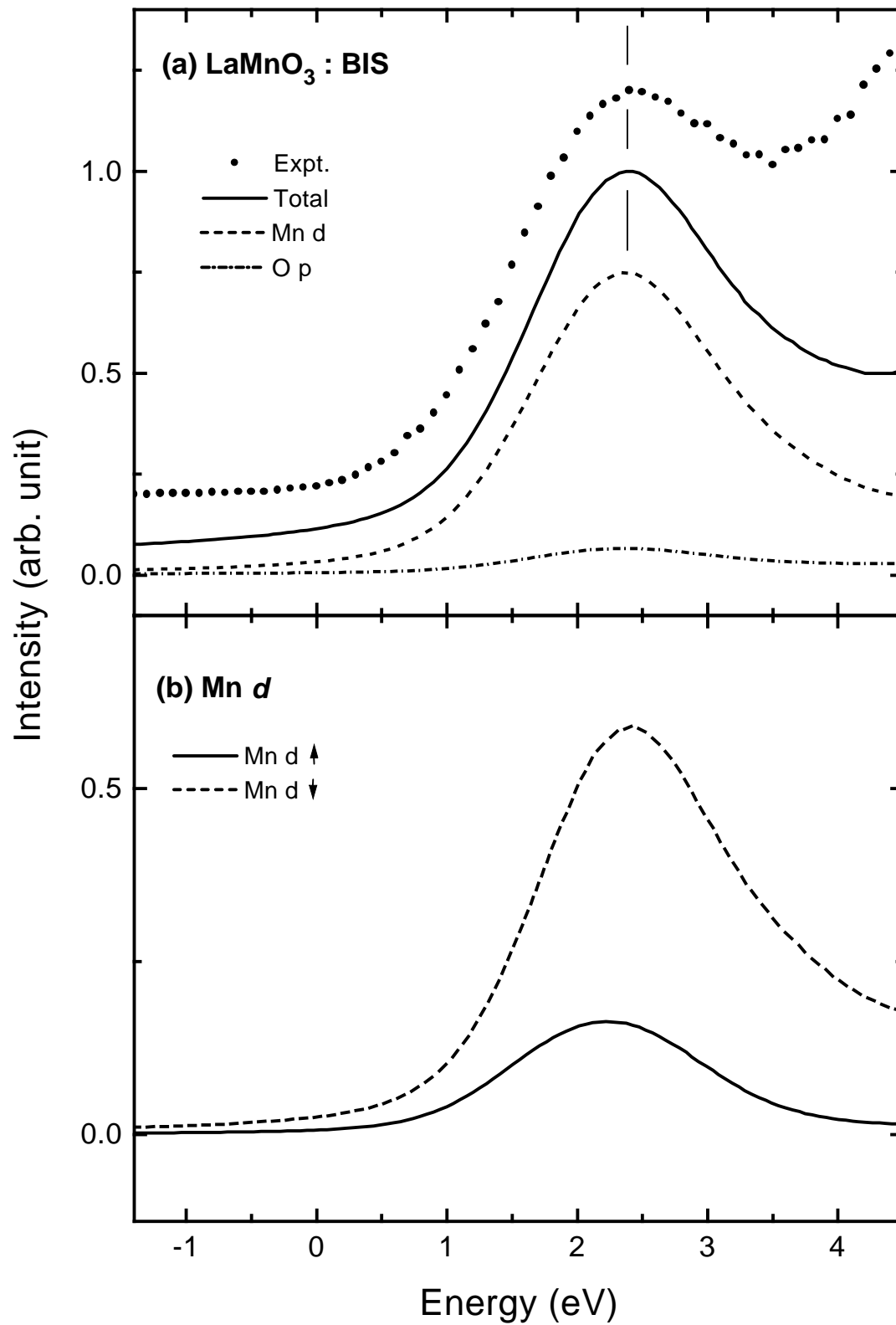
Sarma *et al.* Fig. 2



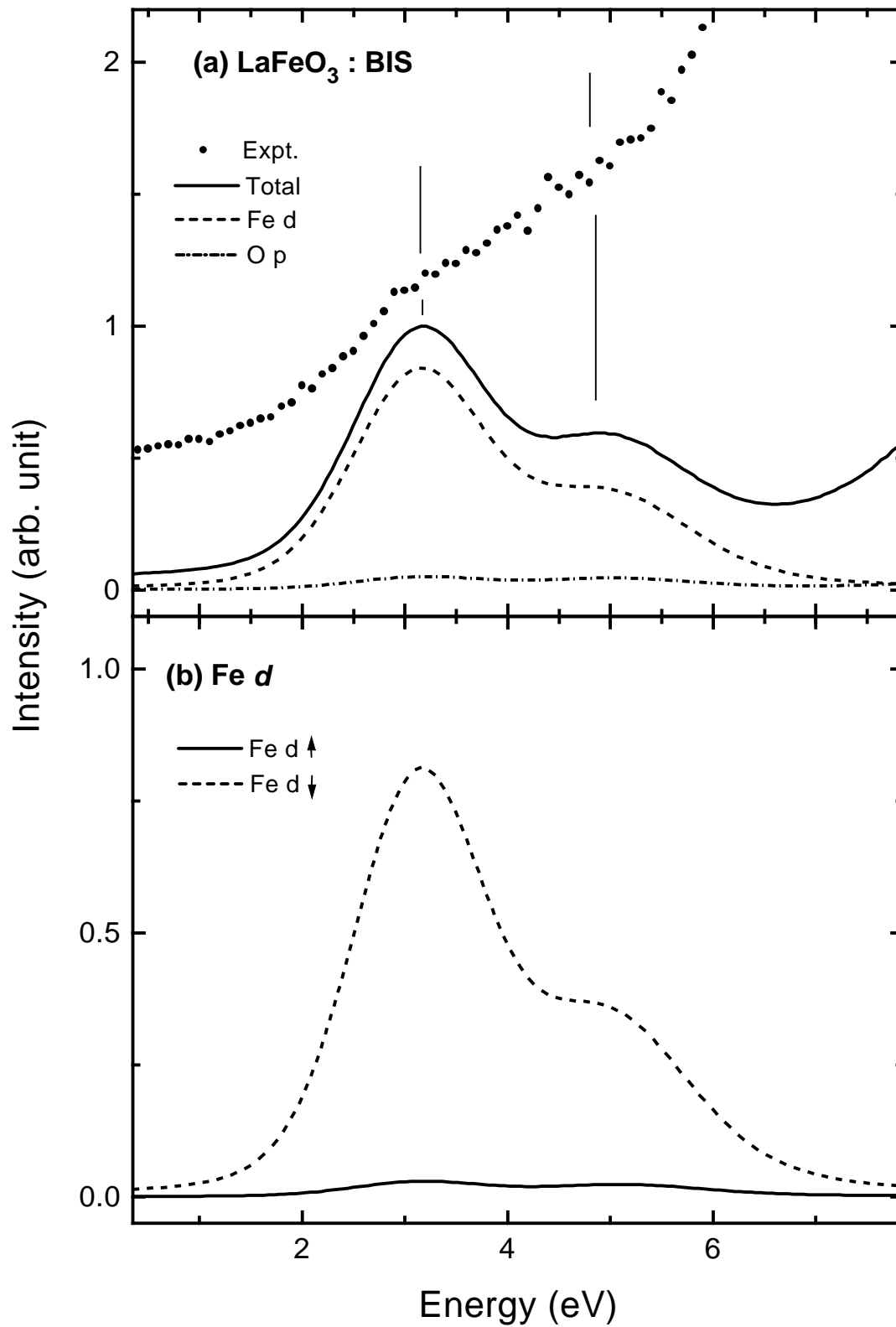
Sarma *et al.* Fig. 3



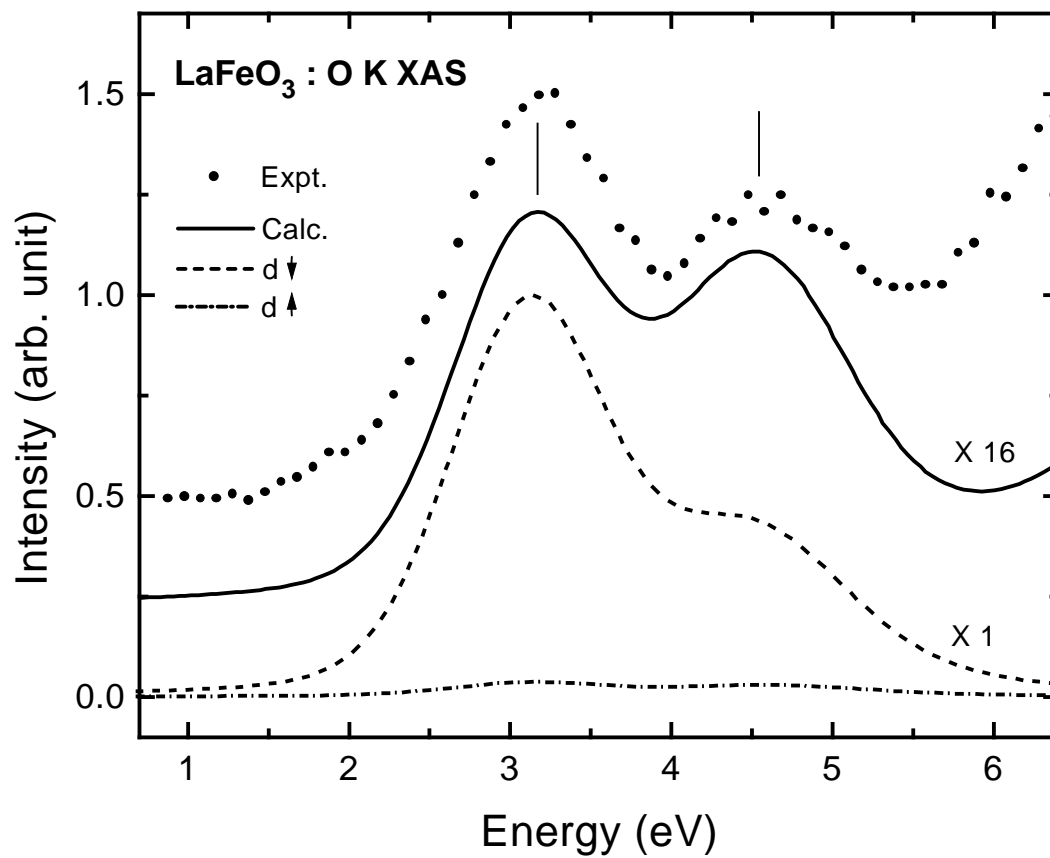
Sarma *et al.* Fig. 4



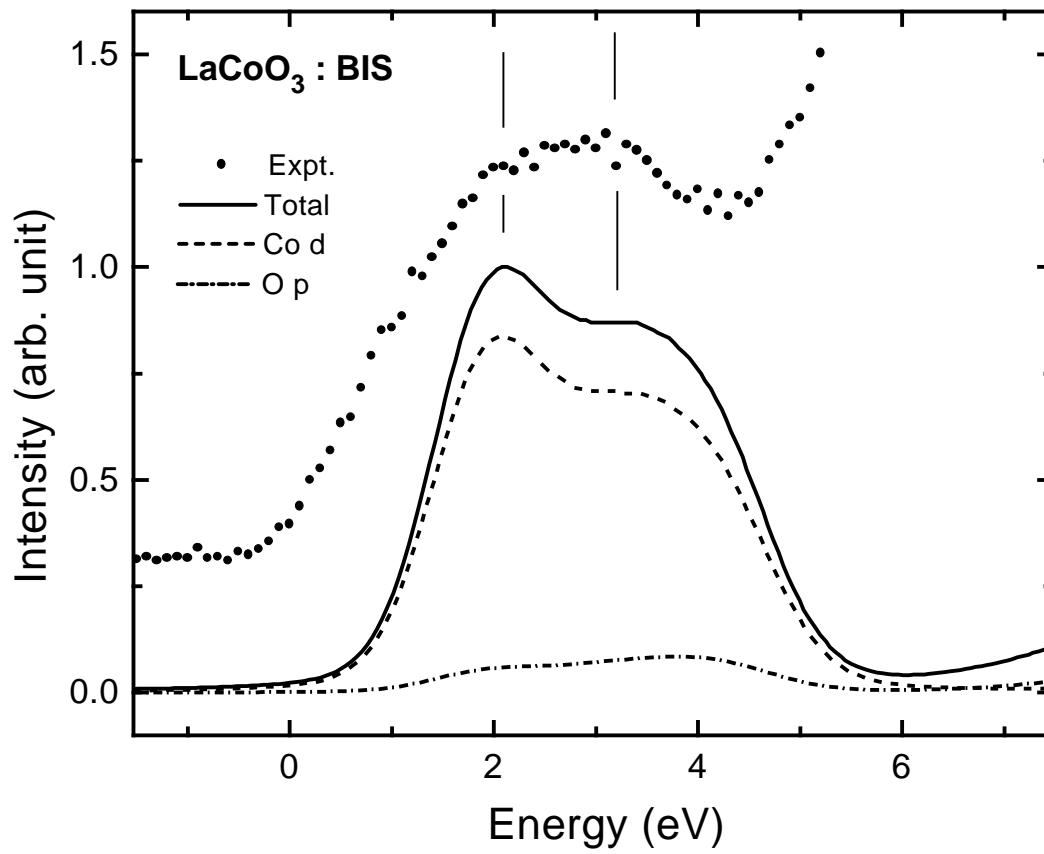
Sarma *et al.* Fig. 5



Sarma *et al.* Fig. 6

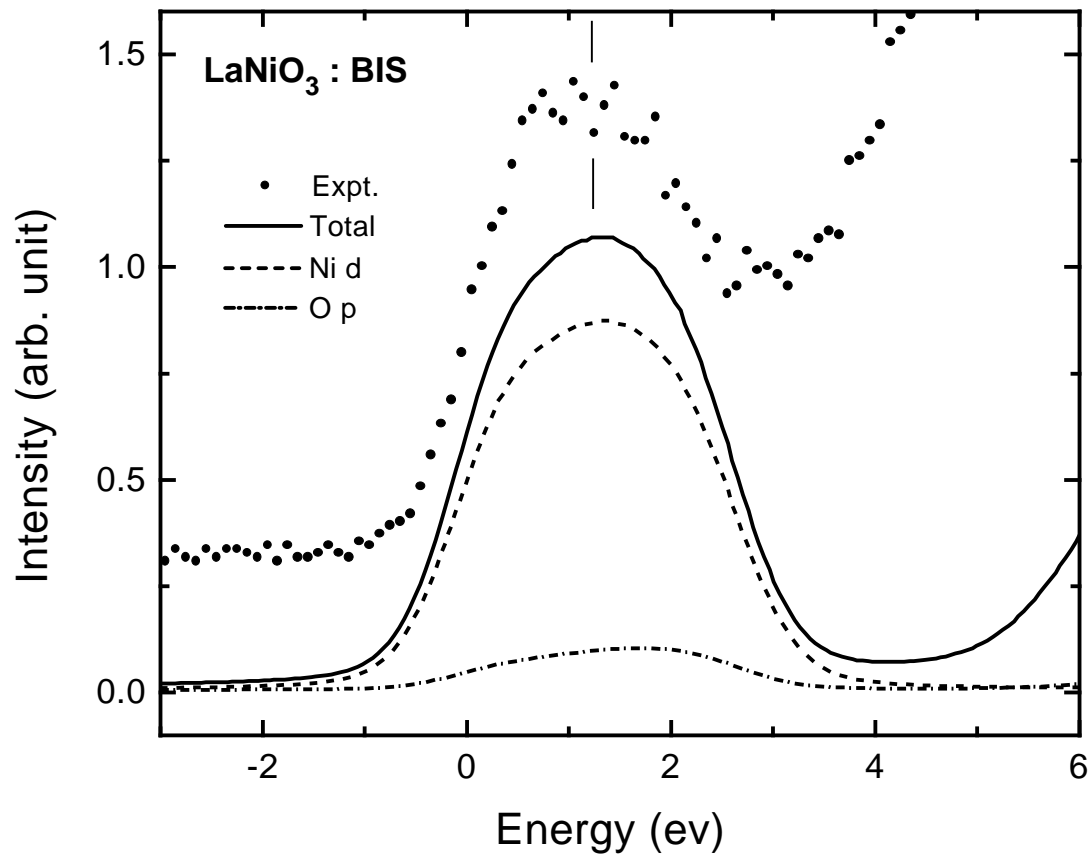


Sarma *et al.* Fig. 7



Sarma *et al.* Fig. 8





Sarma *et al.* Fig. 9